Deformation mechanisms of carbon nanotube fibres under tensile loading by *in situ* Raman spectroscopy analysis

Deformation mechanisms of carbon nanotube fibres under tensile loading by *in situ* Raman spectroscopy analysis

Qiu Li[1], Yi-Lan Kang[1,3], Wei Qiu[1], Ya-Li Li[2], Gan-Yun Huang[1], Jian-Gang Guo[1], Wei-Lin Deng[1] and Xiao-Hua Zhong[2]

[1] Tianjin Key Laboratory of Modern Engineering Mechanics, School of Mechanical Engineering, Tianjin University, Tianjin 300072, People's Republic of China
[2] Key Laboratory of Advanced Ceramics and Machining Technology, Ministry of Education, School of Materials Science and Engineering, Tianjin University, Tianjin 300072, People's Republic of China

E-mail: tju_ylkang@yahoo.com.cn

Abstract
Deformation mechanisms of carbon nanotube (CNT) fibres under tensile loading are studied by means of *in situ* Raman spectroscopy to detect the CNT deformation and stress distributions in the fibres. The G′ band in the Raman spectrum responds distinctly to the tensile stress in Raman shift, width and intensity. The G′ band changes with the tensile deformation of the fibre at different stages, namely elastic deformation, strengthening and damage–fracture. It is deduced that the individual CNTs only deform elastically without obvious damage or bond breaking. The yield and fracture of fibres can be due to the slippage among the CNTs.

(Some figures in this article are in colour only in the electronic version)

1. Introduction

Carbon nanotubes (CNTs) have superior mechanical properties with tensile strength up to 11–63 GPa [1]. They are promising for development into high-strength engineering material with light weight through the assembly of CNTs. However, the mechanical property of such assembled CNT-based materials is, quite often, much lower than expected. For instance, the tensile strength of the CNT fibres falls in the range of only 0.1–9 GPa [2–6], far lower than that of the CNTs. To improve the mechanical performance of CNT fibres, the underlying mechanism of loading deformation needs to be known at the microscopic level.

Micro-Raman spectroscopy can provide valuable information on mechanical properties of materials, as applied for CNTs and their composites [7–14]. Moreover, the detection is noncontact and nondestructive which enables the 'real' state of loading in the materials to be given. Meanwhile, the sensitivity of CNTs to strain can be used as a force sensor. Wagner

et al detected strain/stress distribution around the fibres and the defects of the fibre composite materials [7, 8]. Young *et al* studied the deformation behaviour and heating effects of SWNT/epoxy composites as well as the load transfer inside the double-walled CNTs (DWCNTs) of composites [9, 10]. Moreover, Ma *et al* studied the microstructural deformation process of CNT macroarchitectures and composites [11, 12]. However, most of the previous studies address CNT composites rather than pure CNT fibres.

In this work, we have studied the deformation mechanism of CNT fibres by *in situ* Raman spectroscopy. Responses of the Raman band (G′) during the whole stages of tensile deformation have been detected and analysed in correlation with the strain–stress curves. The loading and deformation in CNTs are interpreted from the Raman band changes. The mechanism of fractures is discussed.

2. Materials and methods

The CNT fibres used for the measurements were spun by the chemical vapour deposition spinning process [15]. The

---

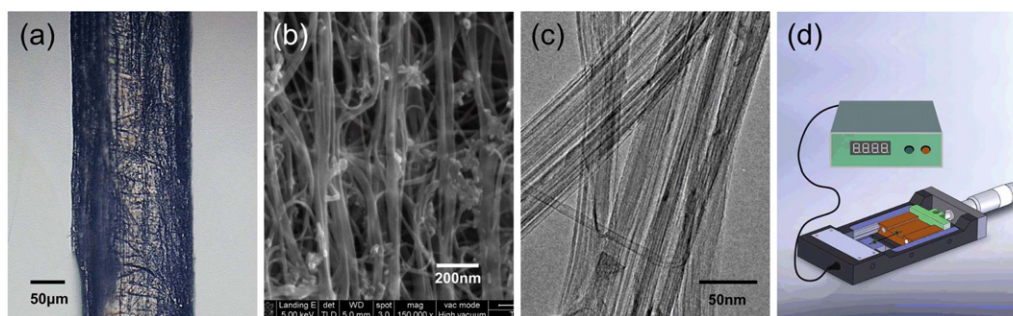[3] Author to whom any correspondence should be addressed.

Figure 1. The macro- and microscopic morphologies of the CNT fibre ((a)–(c)) and a micro-loading device for tensile measurement (d). (a) An optical photo of the CNT fibre. (b) A SEM image observed on the fibre surface. (c) A TEM image of the double-walled CNT bundles in the fibre. (d) A uniaxial tension micro-loading device for CNT fibres.

fibre has a thickness of $\sim$150 μm and consists of bundled DWCNTs interconnected with thinner bundles preferentially aligned along the fibre axis (figures 1(a)–(c)). More detailed information can be found elsewhere [15, 16]. Tensile measurement of the fibre gives a stress–strain curve showing three stages: (I) elastic, (II) strengthening and (III) damage–fracture. The elastic limit is $\sim$0.1 GPa and the strength $\sim$0.3 GPa, in consistency with previous experiments [2–6].

The uniaxial tension operation of the fibres was performed on a precise micro-loading device (figure 1(d)) placed on the analysis platform of a micro-Raman spectroscope (Renishaw InVia Raman spectroscope) [17]. The micro-loading device which is equipped with a screw displacement loading system with precision up to 10 μm, and installed with a micro-force measuring system with precision up to 1 mN, enables the strain and stress of a sample during the tensile process to be given in real-time. The spectroscopic data during the uniaxial tension of the fibres were collected *in situ* by the Raman spectroscope in back scattering configuration under a 632.8 nm He–Ne laser incident light with polarization direction parallel to the fibre axis. The laser is focused on the fibre under an objective of 50$\times$ with a spot of 2 μm in diameter.

3. Results and discussion

The Raman spectra collected *in situ* during tensile deformation of the fibre show distinct changes in the G$'$ band at 2652 cm^{-1}, as shown in figure 2. The G$'$ band is sensitive to stresses as used to detect loading in CNTs [18]. As seen from figure 2, the G$'$ band shifts distinctly towards the lower wavenumbers under loading. Moreover, the edge of the low wavenumbers is broadened. Another change is that the peak intensity increases. The Raman shift, full width at half-maximum (FWHM) and intensity of the G$'$ bands are extracted as shown in figures 3(b)–(d).

The Raman shift of the G$'$ bands during the initial elastic stage (strain $<$ 1%) shows linear change (figure 3(b)). This indicates that most individual CNTs have been loaded at the initial stage, and the initial elastic deformation is mainly governed by the elastic deformation of individual CNTs in the CNT fibre. Under tensile loading, the FWHM of the G$'$ band increases with the strain from 47 to 51 cm^{-1} (figure 3(c)). The broadening of the G$'$ band indicates that the loading on the
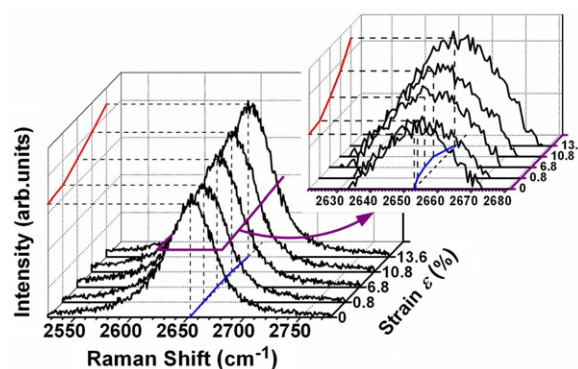

Figure 2. The G$'$ Raman bands of the CNT fibre under typical load conditions. The inset shows the enlarged locality of the G$'$ bands.

CNTs in the fibre is non-uniform. And almost all broadening of the G$'$ band comes from the low-wavenumber edge (inset in figure 2). The asymmetric broadening of the G$'$ band suggests that some of the CNTs in the fibre did not bear any load. This may be one of the reasons why existing CNT fibres have lower elastic modulus.

With the increase of loading to strains of 1%–11.5%, corresponding to the strengthening stage, both the Raman shift change and the FWHM of the G$'$ bands increase only slightly. The data are more scattered. This indicates that the individual CNTs are less deformed compared with the elastic stage. The ratio of the integrated intensities for the D and G bands (I_D/I_G) can be used to determine the defects and damage in the individual CNTs [19, 20]. The values of I_D/I_G are 0.241, 0.243, 0.243, 0.241 at strains of 0, 1%, 5.2%, 13.6%, respectively. The values are almost constant at the different strains. It can be deduced that there is no obvious damage or bond breaking during the tensile loading. The yield of the fibre can be attributed to slippage among CNTs in the fibre. The slippage may also occur between the inner and outer walls of the CNTs. The slippage occurs as a result of the interface stress exceeding the shear limit between the graphite walls in the CNTs. For strain in the range of 0–11.5% (stages I and II), the integrated intensity of the G$'$ bands increases continuously (figure 3(d)). The increase is caused by the aligning of CNT bundles towards the loading direction.

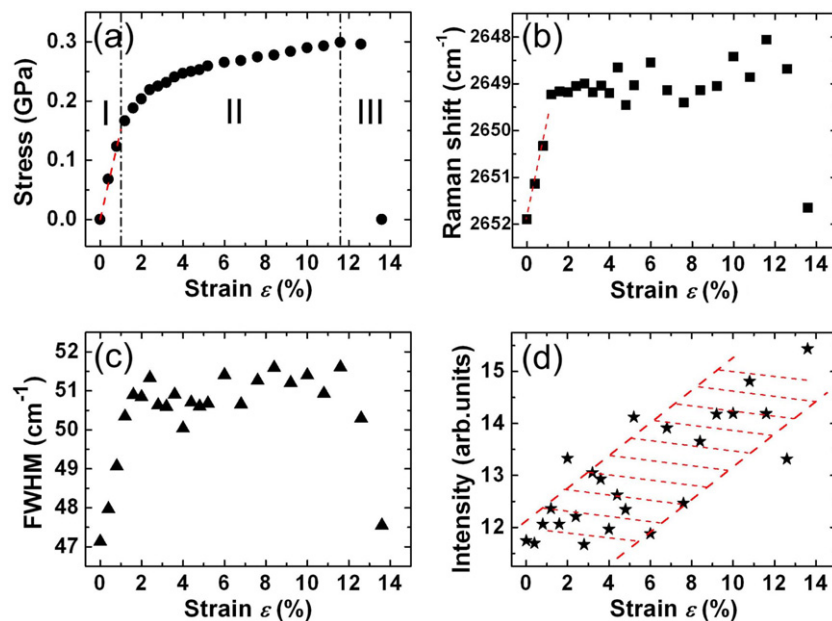Upon fracture, the Raman shift and the FWHM of the G$'$ band reduce back to their initial values (2652 cm^{-1}

Figure 3. The change of both the macroscopic stress (a) and the G′ Raman band information ((b)–(d)) of the CNT fibre with the strain. The G′ Raman band information is the Raman shift (b), the full width at half-maximum (FWHM) (c) and the integrated intensity (d).
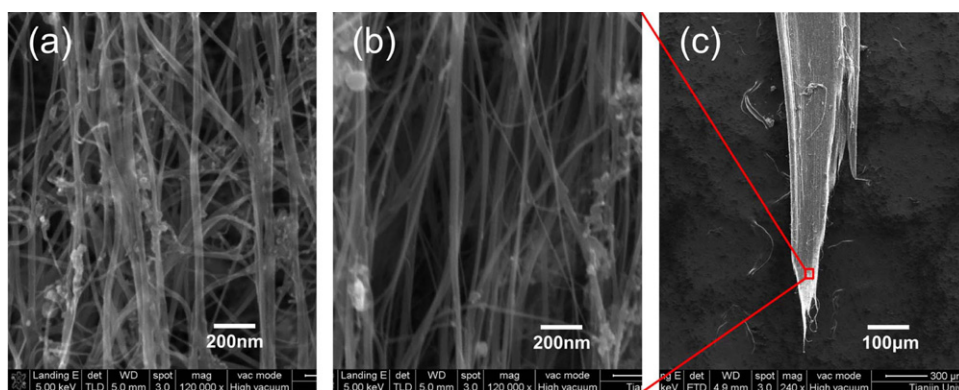

Figure 4. SEM images showing the microstructure of a CNT fibre before tensile loading (a) and after fracture (b), and the fracture morphology of it (c).

and 47 cm^{-1}, respectively) before tensile loading. This indicates that the CNTs have been completely unloaded and the deformation recovered. The recovery of the signals confirms the stress-induced changes in the CNT deformation, and the elastic nature of it. The integrated intensity remains high after the fibres are broken and does not recover to the initial value before tensile loading. This suggests that the fibre keeps the alignment of the CNTs after failure. The fracture of the fibre can be attributed to the accumulation of the slippage.

The Raman results are consistent with SEM observation. Compared with the observations before tensile loading (figure 4(a)), almost all the CNT bundles are straight and aligned along the loading direction after the fibres are broken (figure 4(b)). The average diameter of the CNT bundles in the fibre before tensile loading is ∼23 nm, and that near the breakage after loading is ∼14 nm. The thinning down of the CNT bundles indicates that slippage has occurred among

the CNTs. Moreover, the fractured fibre end is not smooth (figure 4(c)). This suggests the sliding failure of the fibre.

The Raman response under loading–unloading–reloading was also measured, as shown in figure 5. The test was performed by stretching the fibre to a strain of 4.4% (stress 0.23 GPa), then unloading till zero stress, and finally reloading until the fibre broke. As shown in figure 5(a), there is a residual strain of ∼3.4% after completely unloading. Upon reloading, the elastic limit (yield strength) of the fibre increases by 50% and the elastic modulus increases slightly. The variation of the Raman shift for G′ bands with nominal stress is plotted in figure 5(b), which shows a linear change. This provides further information on the elastic nature of the deformation in CNTs under tensile loading, and plastic deformation in them is not obvious. The residual strain can be due to the slippage among CNTs and the unrecoverable part of the CNT alignment during the strengthening stage. The change of the intensity of
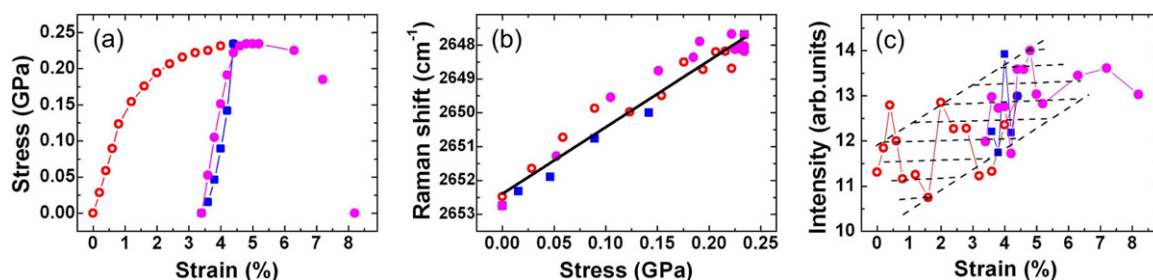
Figure 5. The mechanical response of the CNT fibres during the loading (open red circles), unloading (filled blue squares) and reloading (filled magenta circles) process. (a) The change of the stress with the strain. (b) The change of the Raman shift of G′ bands with the stress. (c) The change of the integrated intensity of the G′ bands with the strain.

the G′ bands with the strain (figure 5(c)) indicates that CNT alignment in the fibre enhances during the first loading and the alignment only partially restores after unloading in the strengthening stage. Thus, when reloading occurs, the number of CNTs bearing the loading increases to more than at the beginning of the first loading, leading to the increase in the elastic modulus and the elastic limit.

4. Conclusions

Overall, *in situ* Raman spectroscopy has been effectively applied to study the deformation behaviour of a CNT fibre under tensile loading by extracting information on the Raman shift, FWHM and intensity. It is discovered that although the macroscopic mechanical response of the fibre shows the different stages of elastic, strengthening and damage–fracture, there is only elastic deformation inside the CNTs with no obvious damage or bond breaking. The yield of the fibres is mainly induced by the slippage among CNTs, whereas fracture is mainly caused by the accumulation of slippage. So it could be concluded that the strength of the CNT fibres is mainly governed by the interface characteristics among CNTs. To make full use of the superior mechanical properties of CNTs in fibres, efforts may be worthwhile to enhance the shear strength of the interfaces between the graphite walls of the different CNTs.

Acknowledgments

References

[1] Yu M F, Lourie O, Dyer M J, Moloni K, Kelly T F and Ruoff R S 2000 *Science* **287** 637
[2] Vigolo B, Penicaud A, Coulon C, Sauder C, Pailler R, Journet C, Bernier P and Poulin P 2000 *Science* **290** 1331
[3] Zhu H W, Xu C L, Wu D H, Wei B Q, Vajtai R and Ajayan P M 2002 *Science* **296** 884
[4] Li Y L, Kinloch I A and Windle A H 2004 *Science* **304** 276
[5] Kozio K, Vilatela J, Moisala A, Motta M, Cunniff P, Sennett M and Windle A 2007 *Science* **318** 1892
[6] Liu K, Sun Y H, Zhou R F, Zhu H Y, Wang J P, Liu L, Fan S S and Jiang K L 2010 *Nanotechnology* **21** 045708
[7] Zhao Q, Wood J R and Wagner H D 2001 *Appl. Phys. Lett.* **78** 1748
[8] Zhao Q and Wagner H D 2003 *Composites* A **34** 1219
[9] Kao C C and Young R J 2004 *Compos. Sci. Technol.* **64** 2291
[10] Cui S, Kinloch I A, Young R J, Noe L and Monthioux M 2009 *Adv. Mater.* **21** 3591
[11] Ma W J *et al* 2009 *Adv. Mater.* **21** 603
[12] Ma W J *et al* 2009 *Nano Lett.* **9** 2855
[13] Qiu W, Kang Y L, Lei Z K, Qin Q H and Li Q 2009 *Chin. Phys. Lett.* **26** 080701
[14] Hadjiev V G, Iliev M N, Arepalli S, Nikolaev P and Files B S 2001 *Appl. Phys. Lett.* **78** 3193
[15] Zhong X H, Li Y L, Liu Y K, Qiao X H, Feng Y, Liang J, Jin J, Zhu L, Hou F and Li J Y 2010 *Adv. Mater.* **22** 692
[16] Motta M, Li Y L, Kinloch I and Windle A H 2005 *Nano Lett.* **5** 1529
[17] Lei Z K, Kang Y L and Qiu W 2008 *CN Patent* 200810053500.6
[18] Cronin S B, Swan A K, Unlu M S, Goldberg B B, Dresselhaus M S and Tinkham M 2005 *Phys. Rev.* B **72** 035425
[19] Lachman N, Bartholome C, Miaudet P, Maugey M, Poulin P and Wagner H D 2009 *J. Phys. Chem.* C **113** 4751
[20] Murakami T, Sako T, Harima H, Kisoda K, Mitikami K and Isshiki T 2004 *Thin Solid Films* **464–465** 319